Publication P1

Kristjan Tabri, Joep Broekhuijsen, Jerzy Matusiak, and Petri Varsta. 2009. Analytical modelling of ship collision based on full-scale experiments. Marine Structures, volume 22, number 1, pages 42-61.

Marine Structures 22 (2009) 42–61

Contents lists available at ScienceDirect

Marine Structures

journal homepage: www.elsevier.com/locate/marstruc

Analytical modelling of ship collision based on full-scale experiments

Kristjan Tabri [a,*,1], Joep Broekhuijsen [a], Jerzy Matusiak [b], Petri Varsta [b]

[a] Schelde Naval Shipbuilding, P.O. Box 555, 4380 AN Vlissingen, The Netherlands
[b] Helsinki University of Technology, Ship Laboratory, P.O. Box 5300, 02015 TKK, Finland

Keywords:
Ship collisions
Full-scale experiments
External dynamics
Water sloshing
Elastic bending of hull girder

A B S T R A C T

This paper presents a theoretical model allowing us to predict the consequences of ship–ship collision where large forces arise due to the sloshing in ship ballast tanks. The model considers the inertia forces of the moving bodies, the effects of the surrounding water, the elastic bending of the hull girder of the struck ship, the elasticity of the deformed ship structures and the sloshing effects in partially filled ballast tanks. The study focuses on external dynamics. Internal mechanics, presenting the collision force as a function of penetration, was obtained from experiments. The model was validated with two full-scale collision experiments, one with a significant sloshing effect and the other without it. The comparison of the calculations and the measurements revealed that the model predictions were in good agreement, as the errors at the maximum value of penetration were less than 10%.

1. Introduction

Regardless of continuous work to prevent collisions of ships, accidents still happen. Due to serious consequences of collision accidents, it is important to reduce the probability of accidents and to minimize potential damage to ships and to the environment. Better understanding of the collision phenomena will contribute to the minimization of the consequences. This paper describes a mathematical model for ship–ship collision simulations and uses the results of full-scale collision experiments for validation.

* Corresponding author.
E-mail addresses: kristjan.tabri@tkk.fi (K. Tabri), joep.broekhuijsen@schelde.com (Joep Broekhuijsen), jerzy.matusiak@tkk.fi (J. Matusiak), petri.varsta@tkk.fi (P. Varsta).
[1] Currently research scientist in Ship Laboratory of Helsinki University of Technology, Finland.

0951-8339/$ – see front matter © 2008 Elsevier Ltd. All rights reserved.
doi:10.1016/j.marstruc.2008.06.002

Many authors approach the collision problem by separating it to external dynamics and internal mechanics. External dynamics determines ship motions while internal mechanics concentrates on the structural response. One of the earliest reported attempts to predict a ship's response in collisions was made by Minorsky [1]. In his study, the energy absorbed in collision, i.e. the loss of kinetic energy, was based on the momentum conservation. Interaction between the ships and the surrounding water was modelled by the additional inertia force proportional to the increase in the ship's mass due to the surrounding water, i.e. the added mass. Motora et al. [2] investigated the validity of Minorsky's assumption of the constant added mass in a series of model tests. They concluded that this assumption is a reasonable approximation only with a very short-term impact – less than 0.5–1 s. For collisions with a longer duration, the value of the added mass increases and can reach a value equal or even higher than a ship's own mass. This problem was solved by making a clear distinction between two components of the radiation force, one component proportional to the acceleration and the other one related to the velocity. Cummins [3] and Ogilvie [4] investigated the hydrodynamic effects and described the force arising from arbitrary ship motions using unit response functions. Like in the work of Motora et al. [2], these approaches require that the frequency dependent added mass and damping coefficients of a ship are evaluated.

Smiechen [5] proposed a procedure to simulate sway motions in the incremental time domain for central, right-angled collisions. Hydrodynamic forces were considered by impulse response functions. In 1982, Petersen [6] continued using impulse response functions and extended the analysis techniques to consider all the ship motions in the waterplane. Petersen also simulated multiple collisions between two similar ships to investigate the effects of different force penetration curves and collision conditions. These simulations revealed that Minorsky's [1] classical method underestimates the loss of kinetic energy.

Woisin [7] derived simplified analytical formulations for fast estimation of the loss of kinetic energy on inelastic ship collisions by using the constant added mass value. In such collisions, it is assumed that at the end of the collision both ships are moving at the same velocity. A few years later, based on experimental data, Pawlowski [8] described the time dependency of the added mass and presented similar analytical formulations. Pedersen and Zhang [9] also examined the effects of sliding and rebounding in the plane of water surface. Also, Brown et al. [10] described a fast time domain simulation model for the external dynamics and compared the results obtained by different calculation models.

Though there are many tools to predict the outcomes of the collision, they tend to lack a relevant validation. A series of full-scale collision experiments conducted in the Netherlands allow for a deeper understanding of the collision phenomena. As the existing tools have failed to predict the outcomes of the experiments at a sufficient accuracy, a new study on collision interaction was initiated. The goal of the study is to analyze these full-scale experiments and as a result, propose a mathematical description of the phenomena. The analysis of the full-scale measurement data indicated that in order to describe the experiments, the effects of free surface waves, i.e. water sloshing, and the elastic bending of the struck ship hull girder have to be included in the model as well.

This paper concentrates on the external dynamics of the collision and the internal mechanics of the colliding ships, giving the collision force, is obtained from the experimental test data. The behaviour of both ships is described separately and combined by the common collision force based on the kinematic condition. The aim is to simulate ship motions during and immediately after the contact. The analysis is limited to a case in which an unpowered ship collides at the right angle with another ship.

2. Analysis of collision interaction

2.1. Formulation of the collision problem

Colliding ships experience a contact load resulting from the impact between the striking ship and the struck ship. This force induces ship motions, which in turn cause hydromechanic forces exerted by the surrounding water. While the striking ship is handled as a rigid body, the struck ship's motions consist of rigid body motions and the vibratory response of the hull girder. Furthermore, a ship's motions are affected by the sloshing forces arising from the wave action at the free surface in partially filled ballast tanks. The collision situation under the investigation is idealized assuming that

- the striking ship is approaching perpendicular to the struck ship,
- the contact point due to the collision is at the midship of the struck ship,
- the propeller thrust of the ships is zero during the collision,
- the bow of the striking ship is rigid and does not deform,
- the collision force as a function of penetration is known *a priori* and it is independent of the penetration velocity,
- the collision force excites the dynamic bending of the hull girder of the struck ship,
- ballast tanks in both ships are partially filled.

The first two idealizations state that only symmetric collisions are investigated. Consequently, all the motions and forces are on the x_0z_0-plane. Fig. 1 presents collision dynamics with motions and penetration. Here and in the subsequent sections superscript characters A and B denote the striking and the struck ship, respectively. Coordinate systems $x^Ay^Az^A$ and $x^By^Bz^B$ have their origins fixed to the ship's centre of gravity. These coordinate systems are used to describe the motions of the colliding ships relative to an inertial Earth fixed coordinate system $x_0y_0z_0$. At the beginning of the collision, the Earth fixed coordinate system coincides with the $x^Ay^Az^A$ system. Forces acting on the striking ship are denoted as X^A, Z^A and M^A for surge, heave and pitch. For the struck ship, they are Y^B, Z^B and K^B for sway, heave and roll, respectively. All of these forces are acting on a ship coordinate system.

During the contact, the collision force, i.e. the response of the ship structures, is equal to the force required to displace the ship. The collision force thus depends on the ships' motions, and the collision problem is basically formulated with the displacement components. Relative displacement between the striking ship and the struck ship, i.e. the penetration depth,

$$\delta(t) = \int_0^t \left\{ \left[u^A(t) + \dot{\gamma}^A(t)h^A\right]\cos\gamma^A(t) - \left[v^B(t) - \dot{\varphi}^B(t)h^B + \dot{\eta}^B\right]\cos\varphi^B(t) \right\} dt \tag{1}$$

forms the time t dependent kinematic condition for the collision process. Here u^A and $\dot{\gamma}^A$ are the surge velocity and the pitch rate of the striking ship, v^B and $\dot{\varphi}^B$ are the rigid body sway velocity and the roll rate of the struck ship, respectively. Velocity $\dot{\eta}^B$ describes the horizontal vibration response of the hull girder of the struck ship. The vertical distance between the ship's centre of gravity and the collision point is denoted by h^A and h^B. It should be noted that Eq. (1) assumes small rotational motions. All of these motion components depend on the forces acting on the ships. The following sections present the formulations, where the outcome will be the time history of the penetration validated with the measured one.

2.2. Hydromechanic forces and moments

Hydromechanic forces and moments acting on a floating object consist of water resistance, hydrostatic restoring forces and radiation forces expressed in terms of hydrodynamic damping and

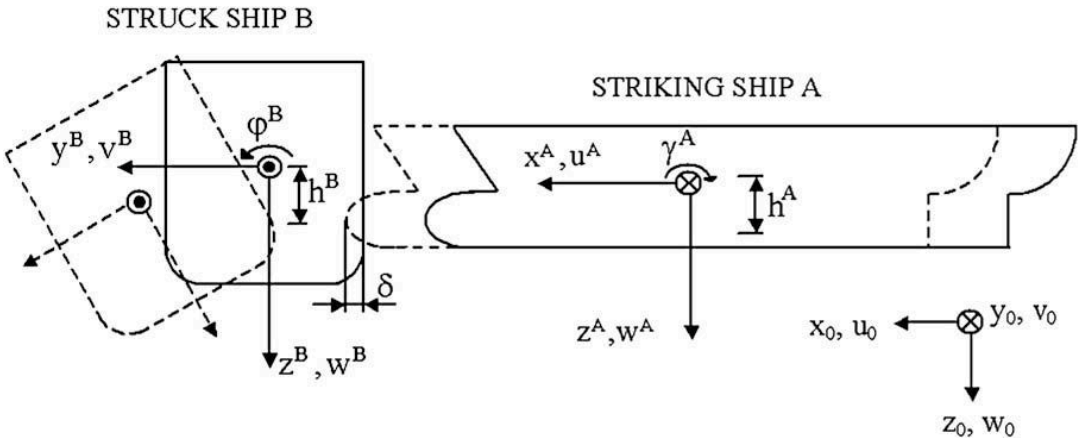

Fig. 1. Coordinates used in the analysis.

added mass. A ship moving in water encounters frictional and residual resistances. Residual resistance is not included in the study because it is considered small compared to other phenomena. Frictional water resistance is approximated with the ITTC-57 friction line formula.

Hydrostatic restoring forces exerted on the ship are proportional to its displacement from the equilibrium position. Linear dependency between the displacement and the resultant force is given by a constant spring coefficient. This simplification holds when the displacements from the equilibrium position are small.

It is a common practice to model the radiation forces by the added mass and damping coefficients. These coefficients are frequency dependent. In the frequency domain, the force due to acceleration $\dot{v}$ and velocity v is evaluated as

$$F_{\mathrm{H}}(\omega) = -a(\omega)\dot{v}(\omega) - b(\omega)v(\omega), \tag{2}$$

where $a(\omega)$ and $b(\omega)$ are the added mass and damping coefficients. For the sake of brevity and clarity a single translational degree of freedom motion is considered here. However, this representation applies for six degrees of freedom when discussing the radiation forces. Eq. (2) is only valid in the case of pure harmonic motion. Therefore it does not suit well for the time domain simulations with arbitrary motions. To represent the radiation forces in the time domain, it is useful to split them into a part F_μ proportional to the acceleration and a velocity dependent damping part F_K:

$$F_{\mathrm{H}}(t) = F_\mu(t) + F_K(t). \tag{3}$$

The force proportional to the acceleration is calculated as

$$F_\mu(t) = -\mu\rho\nabla\dot{v}(t), \tag{4}$$

where

$$\mu = \lim_{\omega\to\infty}\frac{a(\omega)}{\rho\nabla}. \tag{5}$$

Force F_μ given by Eq. (4) would almost be the full representative of the radiation forces if the duration of the motion is short. If the duration exceeds 0.5–1 s, damping starts to play a role [2]. This is considered by force F_K. In the time domain, this force is represented by the so-called convolution integral [3].

$$F_{\mathrm{K}}(t) = -\int_0^t K(\tau)v(t-\tau)\mathrm{d}\tau, \tag{6}$$

where $K(\tau)$ is a retardation function, taking into account the memory effect of the force:

$$K(\tau) = \frac{2}{\pi}\int_0^\infty b(\omega)\cos(\omega\tau)\mathrm{d}\omega. \tag{7}$$

Retardation functions were evaluated by the Fast Fourier Transformation algorithm, as described by Matusiak [11].

For the rotational motions the moments of added mass and damping coefficients are used instead of their linear motion counterparts. Also the corresponding rotational accelerations and velocities are used.

As the full-scale experiments were carried out in relatively shallow water, the effect of the depth of water on the frequency dependent coefficients was investigated. For comparison, the coefficients were evaluated by the Frank close-fit theory [12] and by the finite element (FE) method based on the two-dimensional linear potential theory [13]. In Frank's theory, the velocity potential has to fulfill the Laplace equation in the whole fluid domain and the boundary conditions at the free surface, at the body surface and infinitely far away from the body. The FE method fulfils additional boundary conditions at the bottom of the sea, thus the effects of shallow water are included. For comparison, the coefficients are calculated for a two-dimensional rectangular cylinder with the breadth to draught ratio $B/T = 4.4$ and the water depth to draft ratio $h/T = 2.8$.

Effects on the waterplane motion components like surge, sway and roll were small. The most significant increase in the added mass and damping values can be seen in the coefficients of heave motion, see Figs. 2 and 3. As in the experiments analyzed later, the prevailing motion components were surge and sway, Frank's theory was considered sufficient.

2.3. Water sloshing in partially filled tanks

Sloshing is a violent flow inside a fluid tank with a free surface. Sloshing is induced if the tank's motions are in the vicinity of some of the natural periods of the fluid motion inside the tank. Several numerical methods have been developed to calculate such fluid-structure interaction, but their disadvantage is a long computational time. For convenience, it may be desirable to replace the fluid by a simple mechanical system. This section describes a mechanical system that produces the same forces as the sloshing fluid.

In a simplified mechanical model, sloshing water is replaced with a number of oscillating masses. According to the potential theory, a complete mechanical analog for transverse sloshing must include an infinite number of such masses. It has been shown by the analysis that the effect of each spring-mass element decreases rapidly with the increasing mode number [14]. The sufficient number of mass-spring elements is evaluated by comparing the results with those obtained by computational fluid dynamics (CFD). Fig. 4 presents the idea behind the equivalent mechanical model.

The effect of sloshing is considered only in the case of horizontal motions. Sloshing effects on the rotational motions could be incorporated by evaluating the equivalent height h between the fluid centre of gravity and the mass-spring element, including their effects at the equilibrium of the moment.

Every eigenmode of fluid motions inside the tank is represented by one mass-spring element, a damper and one rigid mass. The equation of the translational motion for a single mass m_n connected to the tank walls by a spring of stiffness k_n and a damper with a damping coefficient c_n becomes

$$m_n\ddot{x}_n + c_n(\dot{x}_n - \dot{x}_R) + k_n(x_n - x_R) = 0, \tag{8}$$

in which x_R and x_n present the motions of a rigid mass and those of an oscillating mass in respect to an inertial coordinate system. Here the sloshing damping is described as a viscous damping and the damping force is always proportional to the relative velocity between the oscillating mass and the rigid mass. In reality, sloshing is damped out due to the viscosity of water and due to water impacts on the tank structure. For a precise description of the sloshing, more complicated damping models should be used. As a detailed investigation of the sloshing behaviour exceeds the limits of this study, viscous damping is considered to be a sufficient representative of the phenomenon.

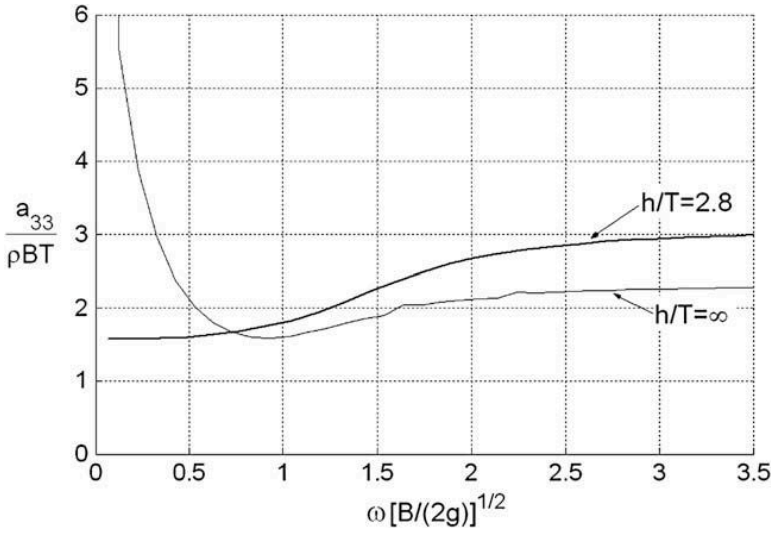

Fig. 2. Effect of shallow water on the heave added mass.

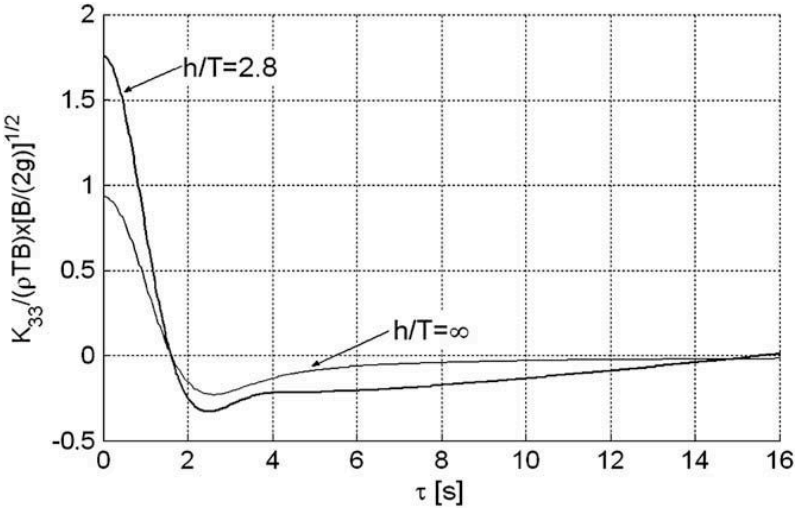

Fig. 3. Effect of shallow water on the heave retardation function.

From Eq. (8), the reaction force of a single oscillating mass to the tank structure is simply $-c_n(\dot{x}_n - \dot{x}_R) - k_n(x_n - x_R)$. The total force F_M acting on the tank structure can be expressed as a sum of the forces due to the rigid mass and the force due to the N oscillating masses

$$F_M = m_R\ddot{x}_R + \sum_{n=1}^{N} m_n\ddot{x}_n. \tag{9}$$

Properties m_n, c_n and k_n for the spring-mass elements were derived so that the mechanical model would give a force identical to the fluid force F_F. The fluid force in a moving tank was obtained by integrating the pressure over the tank boundaries

$$F_F = \oint_S p(x,y,z,t)\mathrm{d}S. \tag{10}$$

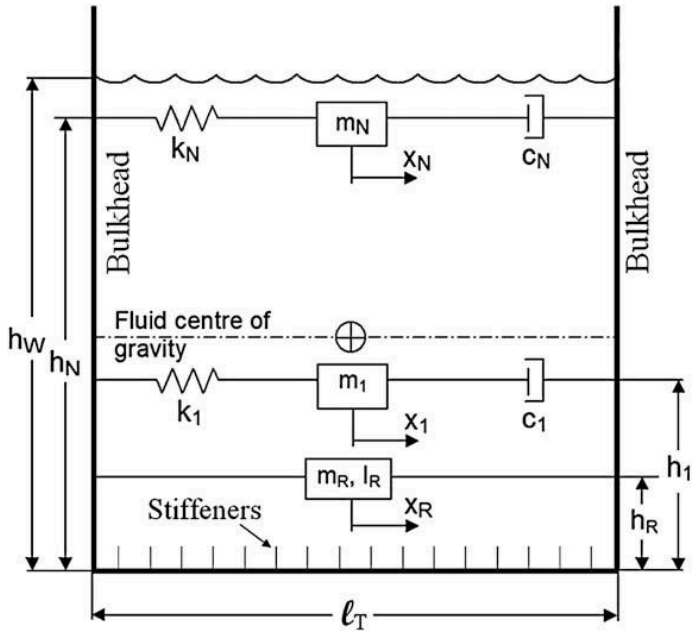

Fig. 4. Simplified mechanical model for sloshing.

Pressure distribution $p(x,y,z,t)$ for an irrotational flow of inviscid and incompressible fluid is obtained from Bernoulli's equation using the concept of velocity potential. The velocity potential is evaluated by satisfying the Laplace equation, the kinematic body boundary condition, the linearized kinematic and dynamic free surface boundary conditions.

Given the formulations for F_M and F_F, the properties m_n, c_n and k_n were evaluated by the equilibrium of the forces. Refs. [15] and [14] present lengthy derivations and give formulations for m_n and k_n. Total fluid mass m_T in a tank with breadth B and fluid height h_W is divided into N oscillating masses and into a single rigid mass

$$m_R = m_T - \sum_{n=1}^{N} m_n. \tag{11}$$

Sloshing damping was evaluated using the logarithmic decrement of damping δ, defined as a ratio between two successive velocity peaks

$$\delta \equiv \ln \frac{v_i}{v_{i+1}} = \frac{2\pi\xi}{\sqrt{1-\xi^2}}, \tag{12}$$

where ξ is a damping ratio. The logarithmic decrement was evaluated by the CFD calculations. Due to simplicity, in the collision simulations presented later, it is assumed that δ is the same for each mass-spring element. The damping coefficient c_n of the nth mass is

$$c_n = \frac{\omega_n}{\pi}\delta. \tag{13}$$

When a ship with I fluid tanks is under consideration, the total rigid mass $\widehat{m}_R$ of the ship is the sum of the ship structural mass m_{ST} and the rigid part of the fluid mass in each tank. Using Eq. (12), the total rigid mass $\widehat{m}_R$ is

$$\widehat{m}_R = m_{ST} + \sum_{i=1}^{I} m_{R,i} = m_{ST} + \sum_{i=1}^{I}\left(m_{T,i} - \sum_{n=1}^{N} m_{n,i}\right). \tag{14}$$

It follows that the total number of oscillating masses is $J = IN$. The motions of the whole ship can be presented by a system similar to that depicted in Fig. 4. The complete system consists of J oscillating masses and the rigid mass $\widehat{m}_R$. If such a system is subjected to an external excitation force F_E acting on the rigid mass, the equation of motion combining Eqs. (8) and (9) is expressed as

$$\begin{bmatrix} \widehat{m}_R & 0 & \cdots & 0 \\ 0 & m_1 & \cdots & 0 \\ \vdots & \vdots & \cdots & \vdots \\ 0 & 0 & \cdots & m_J \end{bmatrix} \begin{Bmatrix} \ddot{x}_R \\ \ddot{x}_1 \\ \vdots \\ \ddot{x}_J \end{Bmatrix} + \begin{bmatrix} \sum_{j=1}^{J} c_n & -c_1 & \cdots & -c_J \\ -c_1 & c_1 & \cdots & 0 \\ \vdots & \vdots & \cdots & \vdots \\ -c_J & 0 & \cdots & c_J \end{bmatrix} \begin{Bmatrix} \dot{x}_R \\ \dot{x}_1 \\ \vdots \\ \dot{x}_J \end{Bmatrix}$$
$$+ \begin{bmatrix} \sum_{j=1}^{J} k_n & -k_1 & \cdots & -k_J \\ -k_1 & k_1 & \cdots & 0 \\ \vdots & \vdots & \cdots & \vdots \\ -k_J & 0 & \cdots & k_J \end{bmatrix} \begin{Bmatrix} x_R \\ x_1 \\ \vdots \\ x_J \end{Bmatrix}$$
$$= \begin{Bmatrix} F_E \\ 0 \\ \vdots \\ 0 \end{Bmatrix}. \tag{15}$$

Matrices in Eq. (15) were composed in a way consistent with the motion definitions of Eq. (8). According to that definition, all the motions are defined with respect to an inertial frame, and the interaction between the rigid body and the oscillating masses is through the damping and stiffness matrices.

The necessary number of oscillating masses per tank and the damping properties were evaluated by comparing the results of the mechanical model with those of the numerical CFD calculations. Two-dimensional (2D) calculations were made applying the CFD program Ansys Flotran with the volume of fluid (VOF) method [16]. The verification was done for a two-dimensional tank with breadth $l_T = 10$ m and water height $h_W = 0.95$ m. To simulate the sloshing comparable to that in the case of the collision experiments analyzed later, two different calculations were carried out as follows:

- For a decelerated tank, with an initial velocity $V_0 = 3.5$ m/s decelerated to zero in 0.5 s. Simulations were carried out with and without transversal stiffeners with a height of 0.3 m. Sloshing direction was transversal to stiffeners.
- For an accelerated tank, with the velocity increasing from zero to the final velocity $V_F = 2.5$ m/s. No stiffeners were modelled.

Fig. 5 presents the sloshing force obtained by the CFD calculations in the case of the decelerated motion. Results show that sloshing is damped out significantly due to the first impact at the tank wall. As a result the amplitude of the sloshing force decreases to almost a quarter of its maximum value. After the first impact, damping decreases and changes in force amplitudes during one period are small.

The effect of the stiffeners in those 2D calculations is not significant and it causes only slight changes in the peak values of the sloshing force. In reality, the effect of the stiffeners is higher, as in 2D CFD calculations the stiffeners at tank sides are not taken into consideration. Furthermore, the effect of the stiffeners increases as the water depth in the tank decreases.

As the contact in real collision is only of a short duration, damping values and the sufficient number of masses are evaluated considering approximately for the first 5 s of the CFD calculations. Fig. 6 presents part of Fig. 5 together with the results of the mechanical model. The thick solid line shows the results of the VOF calculations and thin lines show the results of the mechanical model in the case of different damping coefficients. Our analysis revealed that the damping coefficient $\xi = 0.2\ldots0.3$ is suitable for the decelerated motion.

The analysis of the accelerated tank motions shows that $\xi = 0.05\ldots0.1$ is a suitable damping coefficient. Damping is higher in the case of the decelerated motion, indicating that higher velocity is damped out faster. Also, stiffeners increase damping in the case of the decelerated motion. Still, it should be remembered that those values depend on the velocity and should be reconsidered if the velocities differ from those described above. Furthermore, our analysis revealed that a sufficient number of oscillating masses in a single tank are three.

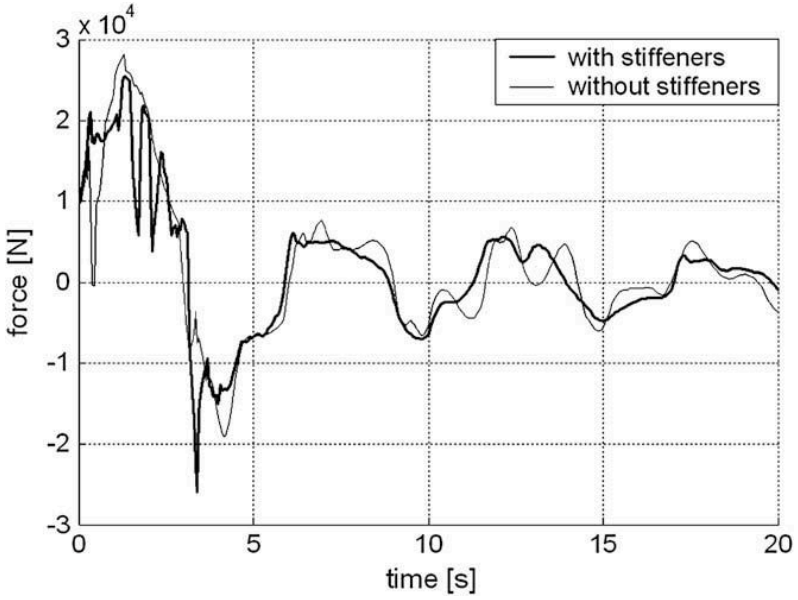

Fig. 5. Sloshing damping analysis with the VOF method for a decelerated tank at an initial velocity of $V_0 = 3.5$ m/s. Sloshing direction transversal to stiffeners.

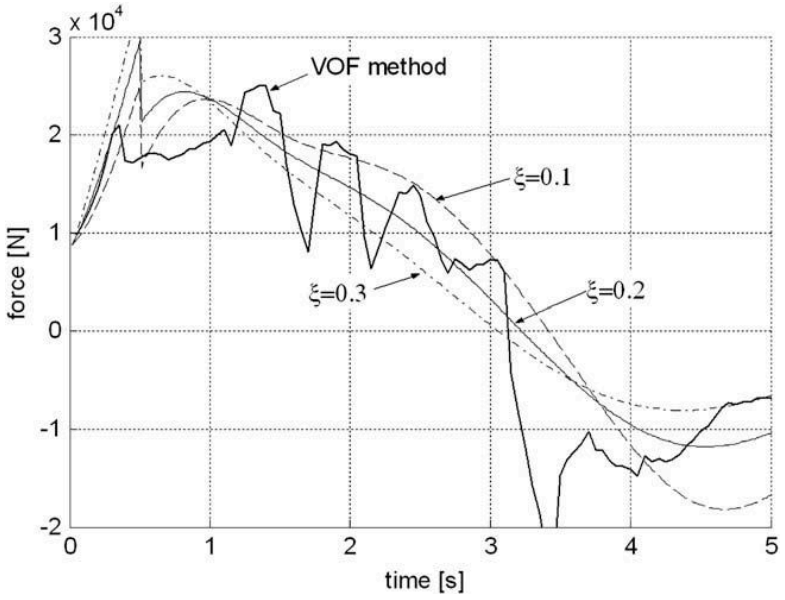

Fig. 6. Evaluation of damping coefficient ξ by comparing the results of the VOF method to those of the mechanical model. Decelerated tank at $V_0 = 3.5$ m/s and $N = 3$. Sloshing direction transversal to stiffeners.

2.4. Elastic bending of a ship hull girder

Impact loading on a ship induces not only the rigid body motions, but also the dynamic bending of the ship hull girder. Dynamic bending covers the hull girder vibration where the cross-sections of the beam remain plane. This allows the modelling of the ship hull as an Euler–Bernoulli beam with the free ends. Major physical properties of the beam are its length L, flexural stiffness $EI(x)$, internal damping ξ, and mass per unit length $m(x)$. The transverse loading $q(x,t)$ is assumed to vary arbitrarily with position and time, and the transverse displacement response $\eta(x,t)$ is also a function of these variables.

The total dynamic response of the ship hull girder is regarded to be a superposition of the responses of the different eigenmodes. The essential operation of the mode-superposition analysis is the transformation from the geometric displacement coordinates to the normal coordinates. This is done by defining the bending response η as

$$\eta(x,t) = \sum_{i=1}^{\infty} \phi_i(x) p(t), \tag{16}$$

which indicates that the vibration motion is of a natural mode $\phi_i(x)$, having a time dependent normal coordinate $p(t)$. Mode shapes and corresponding eigenfrequencies ω_i were evaluated as presented in [17]. The equation of motion for the ith vibratory mode is expressed as in [18]

$$m_i^* \ddot{p}_i(t) + 2\xi\omega_i m_i^* \dot{p}_i(t) + \omega_i^2 m_i^* p_i(t) = q_i^*(t), \tag{17}$$

where the generalized mass of the ith mode is

$$m_i^* = \int_0^L \phi_i(x)^2 m(x) \mathrm{d}x, \tag{18}$$

and the generalized loading associated with the mode shape $\phi_i(x)$ is

$$q_i^*(t) = \int_0^L \phi_i(x) q(x,t) \mathrm{d}x. \tag{19}$$

The value of internal bending damping ξ for ships is usually obtained experimentally. If no empirical values exist for a particular ship, the measured internal damping values from many ships are reported in [19]. These values indicate that the internal damping is practically independent of the frequency and a value $\xi = 0.05$ may be used.

2.5. Contact force

During a collision, both ships experience a common contact force F_C arising from the bending, tearing and crushing of the material in the ship structures. The best way to obtain contact force for highly non-linear process such as a collision is by a sophisticated finite element (FE) analysis or by experimental testing. FE calculations for the contact force exceed the limitations of the paper and are not analyzed here. The emphasis of the study is on the external dynamics and the contact force as a function of penetration is assumed to be known *a priori* from the experimental data or from the other sources. Due to symmetric collisions, only one force-penetration curve is necessary. An example of an experimentally measured force-penetration curve is depicted in Fig. 7 with a solid line. The dotted line shows the fitted curve.

When the collision force reaches its maximum, ships start to separate and the penetration decreases. Due to the elasticity of the deformed structures, contact is not lost immediately and the collision force still has some value. This elasticity, i.e. the elastic spring-back, is modelled by a single variable α, which gives the inclination for the spring-back line. Fig. 7 shows two examples of the spring-back lines, both having the same inclination, but a different starting point. This starting point is equal to the maximum penetration in the collision and its location is determined by the external dynamics. If the penetration starts to increase again after decreasing, the collision force follows the original path.

2.6. Formulations of motion equations

For the sake of brevity, only the equations of motions for the struck ship are presented here in detail. For the striking ship, the equations are simpler as they do not include the component of the vibratory motion. The effect of the bending motion is assumed to be small compared to the rigid body motions and therefore only the first eigenmode is included. Furthermore, only the bending in the sway direction is considered.

It is assumed that the sloshing and the hydromechanic forces are distributed uniformly along the ship length. Concerning the first eigenmode of a uniform beam with free ends, it holds that

$$\int_0^L \phi_1(x)\mathrm{d}x = 0 \tag{20}$$

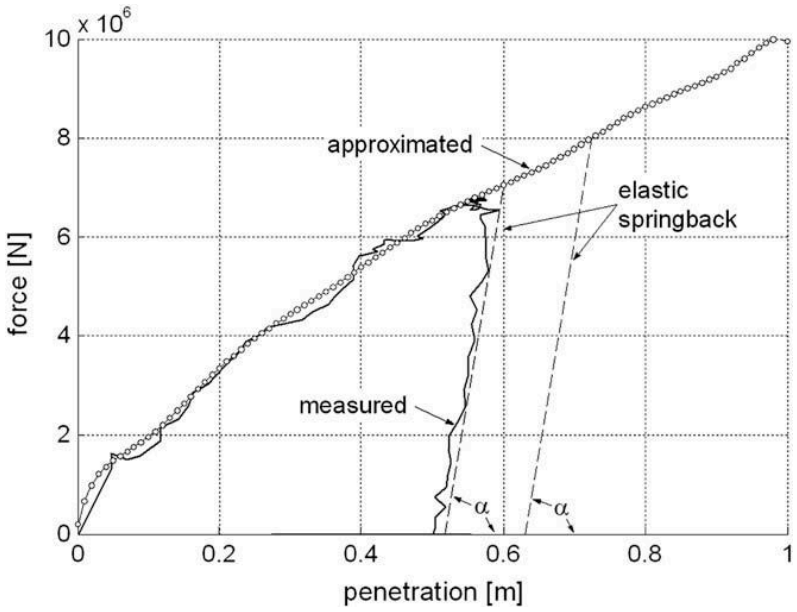

Fig. 7. Measured and approximated force-penetration curve.

and it follows that the uniformly distributed sloshing and hydromechanic forces need not to be included in the bending analysis. Thereby the generalized force for the first eigenmode was evaluated by

$$q_1^{*\mathrm{B}}(t) = \int_0^L \phi_1(x) F_{\mathrm{C}}(x,t)\mathrm{d}x. \tag{21}$$

In reality, those forces are never perfectly uniform. With detailed knowledge available about the distribution of these forces, their effect can easily be included.

A generalized mass $m_1^{*\mathrm{B}}$ was evaluated using the sway added mass μ_{22}^{B} and the total rigid mass $\widehat{m}_{\mathrm{R}}^{\mathrm{B}}$ of the ship as

$$m_1^{*\mathrm{B}} = \int_0^L \phi_i(x)^2 \left(\widehat{m}_{\mathrm{R}}^{\mathrm{B}}(x) + \mu_{22}^{\mathrm{B}}(x)\right)\mathrm{d}x. \tag{22}$$

For convenience, the equations of motions were first evaluated by neglecting the effects of sloshing. Furthermore, assuming that there is no coupling between the motion components and using the notations presented in Fig. 1, the equations were written as

$$\begin{cases} \rho\nabla^{\mathrm{B}}\left(\dot{v}^{\mathrm{B}} - \dot{\varphi}^{\mathrm{B}} w^{\mathrm{B}}\right) = Y^{\mathrm{B}} + \rho g \nabla^{\mathrm{B}} \sin\varphi^{\mathrm{B}} \\ m_1^{*\mathrm{B}}\ddot{p}_1(t) + 2\xi\omega_1^{\mathrm{B}} m_1^{*\mathrm{B}}\dot{p}_1(t) + \left(\omega_1^{\mathrm{B}}\right)^2 m_1^{*\mathrm{B}} p_1(t) = q_1^{*\mathrm{B}}(t) \\ \rho\nabla^{\mathrm{B}}\left(\dot{w}^{\mathrm{B}} + \dot{\varphi}^{\mathrm{B}} v^{\mathrm{B}}\right) = Z^{\mathrm{B}} + \rho g \nabla^{\mathrm{B}} \cos\varphi^{\mathrm{B}} \\ I_x^{\mathrm{B}}\ddot{\varphi}^{\mathrm{B}} = K^{\mathrm{B}}, \end{cases} \tag{23}$$

where ∇^{B} is the volumetric displacement of the ship and I_x^{B} is the moment of inertia with respect to the x-axis. Sway force Y^{B}, heave force Z^{B} and rolling moment K^{B} were described in a ship's coordinate system and were evaluated as the summation of forces and moments described in the previous sections:

$$\begin{aligned} Y^{\mathrm{B}} &= F_{\mathrm{C}} + Y_{\mathrm{F}}^{\mathrm{B}} + Y_{\mathrm{H}}^{\mathrm{B}} \\ Z^{\mathrm{B}} &= Z_{\mathrm{R}}^{\mathrm{B}} + Z_{\mathrm{H}}^{\mathrm{B}} \\ K^{\mathrm{B}} &= F_{\mathrm{C}} h^{\mathrm{B}} + K_{\mathrm{R}}^{\mathrm{B}} + K_{\mathrm{H}}^{\mathrm{B}}, \end{aligned} \tag{24}$$

with subscripts C corresponding to the collision force, F to the frictional resistance, H to the radiation force and R to the hydrostatical restoring force. It should be noted that all the forces due to the surrounding water are included in Y^{B}, Z^{B} and K^{B}. Thus, the added mass does not appear explicitly in Eq. (23), but is included through $Y_{\mathrm{H}}^{\mathrm{B}}$, $Z_{\mathrm{H}}^{\mathrm{B}}$ and $K_{\mathrm{H}}^{\mathrm{B}}$.

In the presence of sloshing, the total mass $\rho\nabla^{\mathrm{B}}$ of the ship was divided into a single rigid mass $\widehat{m}_{\mathrm{R}}^{\mathrm{B}}$ by Eq. (14) and into J^{B} oscillating masses. All the forces and moments presented by Eq. (24) are acting on the rigid mass. Sloshing is induced by the coupling terms in the stiffness and damping matrices in Eq. (15). Furthermore, it is assumed that all the sloshing masses have their centre of gravity at the ship's centre of gravity and therefore they do not contribute to the rotational motions. Denoting motions of the sloshing masses by x^{B}, a new equation of motions is formulated by combining Eqs. (15) and (23), yielding

$$\left[M^{\mathrm{B}}\right]\begin{Bmatrix} \dot{v}^{\mathrm{B}} - \dot{\varphi}^{\mathrm{B}} w^{\mathrm{B}} \\ \ddot{x}_1^{\mathrm{B}} \\ \vdots \\ \ddot{x}_{J^{\mathrm{B}}}^{\mathrm{B}} \\ \ddot{p}_1^{\mathrm{B}}(t) \\ \dot{w}^{\mathrm{B}} + \dot{\varphi}^{\mathrm{B}} v^{\mathrm{B}} \\ \ddot{\varphi}^{\mathrm{B}} \end{Bmatrix} + \left[C^{\mathrm{B}}\right]\begin{Bmatrix} v^{\mathrm{B}} \\ \dot{x}_1^{\mathrm{B}} \\ \vdots \\ \dot{x}_{J^{\mathrm{B}}}^{\mathrm{B}} \\ \dot{p}_1(t) \\ w^{\mathrm{B}} \\ \dot{\varphi}^{\mathrm{B}} \end{Bmatrix} + \left[K^{\mathrm{B}}\right]\begin{Bmatrix} y^{\mathrm{B}} \\ x_1^{\mathrm{B}} \\ \vdots \\ x_{J^{\mathrm{B}}}^{\mathrm{B}} \\ p_1(t) \\ z^{\mathrm{B}} \\ \varphi^{\mathrm{B}} \end{Bmatrix} = \begin{Bmatrix} Y^{\mathrm{B}} + \rho g \nabla^{\mathrm{B}} \sin\varphi^{\mathrm{B}} \\ 0 \\ \vdots \\ 0 \\ q_1^{*\mathrm{B}}(t) \\ Z^{\mathrm{B}} + \rho g \nabla^{\mathrm{B}} \cos\varphi^{\mathrm{B}} \\ K^{\mathrm{B}} \end{Bmatrix}, \tag{25}$$

where

$$\left[M^{B}\right] = \begin{bmatrix} \widehat{m}_{R}^{B} & 0 & \cdots & 0 & 0 & 0 & 0 \\ 0 & m_{1}^{B} & \cdots & 0 & 0 & 0 & 0 \\ \vdots & \vdots & \ddots & \vdots & \vdots & \vdots & \vdots \\ 0 & 0 & \cdots & m_{J^{B}}^{B} & 0 & 0 & 0 \\ 0 & 0 & \cdots & 0 & m_{1}^{*B} & 0 & 0 \\ 0 & 0 & \cdots & 0 & 0 & \widehat{m}_{R}^{B} & 0 \\ 0 & 0 & \cdots & 0 & 0 & 0 & I_{x}^{B} \end{bmatrix} \tag{26}$$

and

$$\left[C^{B}\right] = \begin{bmatrix} \sum_{j=1}^{J^{B}} c_{j}^{B} & -c_{1}^{B} & \cdots & -c_{J^{B}}^{B} & 0 & 0 & 0 \\ -c_{1}^{B} & c_{1}^{B} & \cdots & 0 & 0 & 0 & 0 \\ \vdots & \vdots & \ddots & \vdots & \vdots & \vdots & \vdots \\ -c_{J^{B}}^{B} & 0 & 0 & c_{J^{B}}^{B} & 0 & 0 & 0 \\ 0 & 0 & \cdots & 0 & 2\xi\omega_{1}^{B}m_{1}^{*B} & 0 & 0 \\ 0 & 0 & \cdots & 0 & 0 & 0 & 0 \\ 0 & 0 & \cdots & 0 & 0 & 0 & 0 \end{bmatrix} \tag{27}$$

and

$$\left[K^{B}\right] = \begin{bmatrix} \sum_{j=1}^{J^{B}} k_{j}^{B} & -k_{1}^{B} & \cdots & -k_{J^{B}}^{B} & 0 & 0 & 0 \\ -k_{1}^{B} & k_{1}^{B} & \cdots & 0 & 0 & 0 & 0 \\ \vdots & \vdots & \ddots & \vdots & \vdots & \vdots & \vdots \\ -k_{J^{B}}^{B} & 0 & 0 & k_{J^{B}}^{B} & 0 & 0 & 0 \\ 0 & 0 & \cdots & 0 & \left(\omega_{1}^{B}\right)^{2}m_{1}^{*B} & 0 & 0 \\ 0 & 0 & \cdots & 0 & 0 & 0 & 0 \\ 0 & 0 & \cdots & 0 & 0 & 0 & 0 \end{bmatrix}. \tag{28}$$

For the striking ship, the equations of motion without the effects of sloshing are

$$\begin{cases} \rho\nabla^{A}\left(\dot{u}^{A} + \dot{\gamma}^{A}w^{A}\right) = X^{A} - \rho g\nabla^{A}\sin\gamma^{A} \\ \rho\nabla^{A}\left(\dot{w}^{A} - \dot{\gamma}^{A}u^{A}\right) = Z^{A} + \rho g\nabla^{A}\cos\gamma^{A} \\ I_{y}^{A}\ddot{\gamma}^{A} = M^{A}, \end{cases} \tag{29}$$

where ∇^{A} denotes the volumetric displacement of the ship and I_{y}^{A} denotes the moment of inertia in respect to y-axis. Forces for surge, heave and pitch are

$$\begin{aligned} X^{A} &= F_{C} + X_{F}^{A} + X_{H}^{A} \\ Z^{A} &= Z_{R}^{A} + Z_{H}^{A} \\ M^{A} &= F_{C}h^{A} + M_{R}^{A} + M_{H}^{A}. \end{aligned} \tag{30}$$

The second order differential equations of motion, Eqs. (25) and (29), are non-linear due to the coupling in acceleration terms. Equations can be linearized within a time increment Δt assuming that the changes in the velocities and the time derivatives of the velocities are small within the time increment [6]. Furthermore, all the forces were assumed constant during Δt. Under these assumptions, the solution at the time $(t_0 + \Delta t)$can be found if the solution at the time t_0 is given. Equations were solved using the fourth order Runge–Kutta method.

3. Validation of the theory by full-scale collision experiments

To validate the collision model, the results obtained from a series of full-scale collision experiments were used. Several full-scale collision experiments using two inland vessels have been conducted in the Netherlands by TNO (Dutch Institute for Applied Physical Research) in the framework of a Japanese, German, Dutch consortium of shipyards and a classification society. The experiments conducted had different purposes, such as to validate numerical analysis tools, to investigate various aspects in collision and to prove new structural concepts. In this study, the following two experiments were used to verify the analytical model:

- collision experiments with the *Y*-core side structure.
- collision experiments with the *X*-core side structure.

Those two experiments differ, as in the experiment with the *Y*-core ship side structure, both ships contained large amounts of ballast water and therefore the effects of sloshing were significant. In the experiment with the *X*-core side structure, sloshing effects were practically removed, as only a small amount of ballast water had a free surface.

3.1. Experiment with the Y-core test-section

The experiment with the patented *Y*-core test section designed by Schelde Naval Shipbuilding was conducted in the Netherlands on 9th of July 1998. A detailed description of the collision experiment with a preliminary analysis is presented in [20].

Two moderate size inland waterway tankers were used in the collision test. The striking ship was named Nedlloyd 34 and the struck ship was called Amatha. The main dimensions of both ships are given in Table 1. In the table and in the following figures, subscript 11 corresponds to the surge motion and 22 to the sway motion.

The striking ship, which was equipped with a rigid bulbous bow, impacted the struck ship at amidships on the course perpendicular to the struck ship. Due to that, very small yaw motions were expected. At the moment of the first contact, the velocity of the striking ship was 3.51 m/s.

A comparison between the measured and the calculated results is presented in Figs. 8–11. Figures also include the calculations, where the effects of sloshing are neglected. The time history of the collision force presented in Fig. 8 shows a good agreement at the beginning of the collision. The first force peak is predicted at good accuracy both in terms of the absolute value and the duration. After the first force impulse, the ships separated and the force decreased to zero. Due to a higher resistance of the struck ship and due to the sloshing effects, a second contact occurred. The calculation model predicts the absolute value of the second force peak, but delays it for 0.5 s. In the experiment, also a third contact occurred, which was not predicted by the calculations. The first peak becomes higher and the subsequent contacts do not occur when the sloshing effects are neglected.

Velocities of the ships are presented in Figs. 9 and 10. The general behaviour of the striking ship velocity was the same in the experiment and in the calculation. In the beginning, the velocity decreased

Table 1
Main dimensions and loading conditions of the ships

	Striking ship	Struck ship
Length, L	80 m	80 m
Beam, B	8.2 m	9.5 m
Depth, D	2.62 m	2.8 m
Draft[a], T	1.45 m	2.15 m
Displacement, Δ	774 tons	1365 tons
Added mass of prevailing motion component	$\mu_{11} = 0.05$	$\mu_{22} = 0.24$
Number of tanks	2×5	2×6
Ballast water with free surface	303.5 tons	545.0 tons

[a] In the report [20], the exact draft of the ships is not given, it only contains their total displacements. The draft presented here is evaluated by lines drawings and the reported displacements.

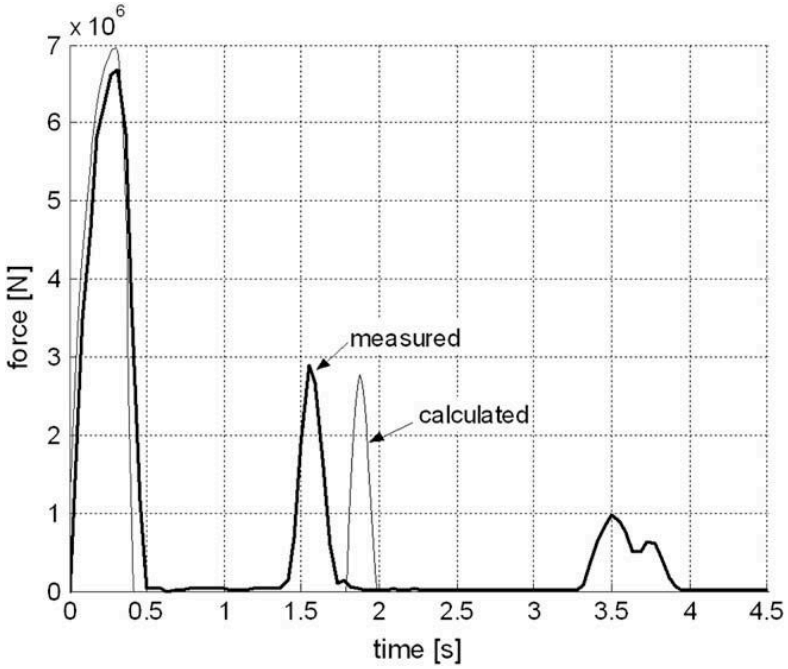

Fig. 8. Collision force F_C as a function of time.

significantly due to the contact force. When the collision force decreased to zero, the ship started to accelerate. This acceleration is mainly due to sloshing, as the sloshing force is preceded by the collision force, see Figs. 6 and 8. In the calculations, the velocity decreases to 0.2 m/s instead of 0.65 m/s, which was measured in the experiment. The calculations with different sloshing properties revealed that the duration of the deceleration is strongly dependent on the sloshing damping coefficient ξ. As the same damping coefficient was used for every tank, regardless of the water height, the source of the inaccuracy is obvious. The second decrease in the velocity, indicating the beginning of the second collision, is also delayed, which in turn results in a delayed second force peak in Fig. 8. When the sloshing is neglected, the ship deceleration is similar to the experimentally measured, but the acceleration is significantly lower. Here the acceleration is only due to the surrounding water, which effect is low compared to that of the sloshing.

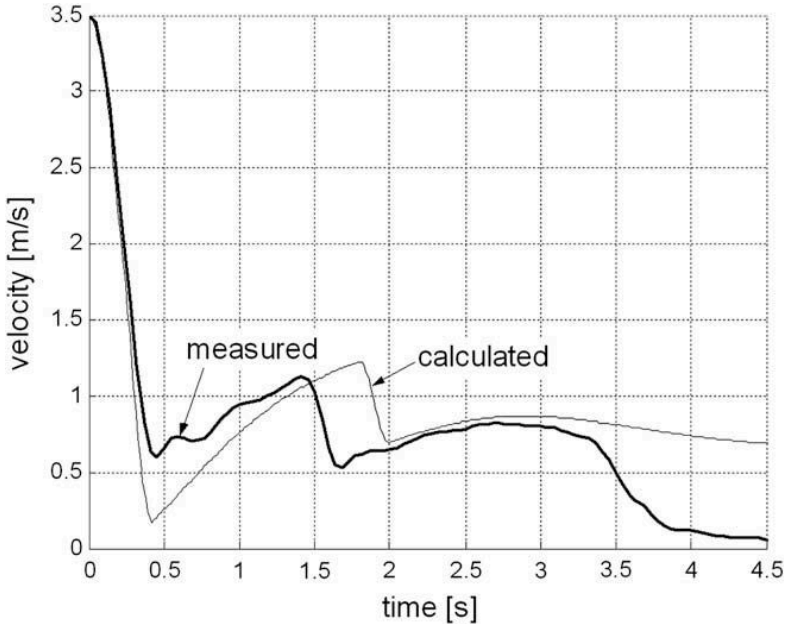

Fig. 9. Velocity of the striking ship.

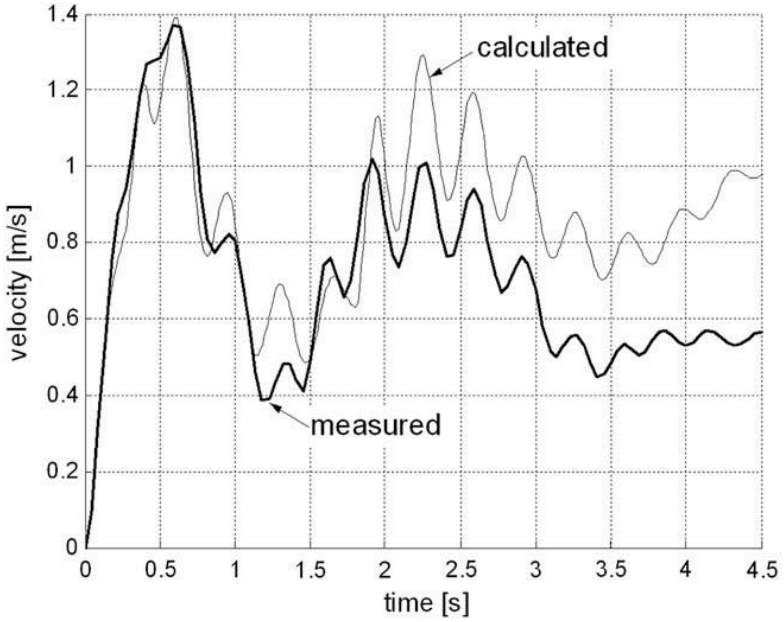

Fig. 10. Velocity of the struck ship.

The time history of the struck ship velocity is presented in Fig. 10. The agreement between the measurement and the calculation is better than in the case of the striking ship. This is mainly due to the fact that in the case of the struck ship, the effects of sloshing were smaller and the changes in the sloshing damping values did not appear so significant. Differences between the measured and the calculated value increased after the second collision, but the general behaviour still remained the same. Again, the sloshing effects are obvious. Without sloshing, the first velocity peak is higher and as there are no subsequent contacts, the velocity remains oscillating around constant level. By the end of the observed time period, the energy involved in the sloshing is almost fully transformed to the kinetic energy of the ship, see Fig. 13, and the calculated velocities approach to each other.

Due to the bending of the ship hull girder, the velocity signal has an oscillatory behaviour. Those oscillations, especially the frequency, are predicted well with the Euler–Bernoulli beam theory. It

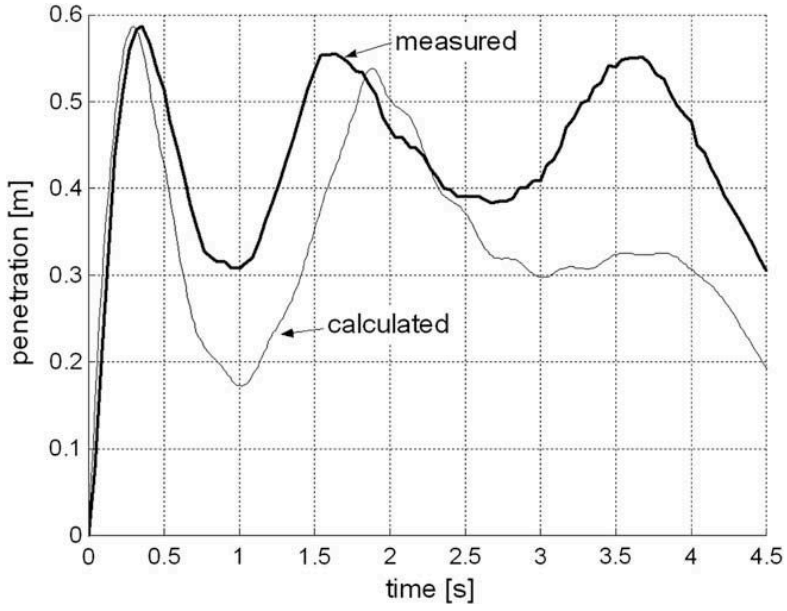

Fig. 11. Penetration as a function of time.

also indicates that the added mass value for the sway motion can be predicted well with Frank's method.

The integration of the relative velocity between the ships results in a penetration time history presented in Fig. 11. Similar effects, which were also seen in the force and velocity time histories, are seen in the penetration value as well. The maximum penetration value determining the damage in the struck ship is predicted with a very good accuracy. After the first peak, the penetration, decreasing too much, also delays. Reasons for that lie in the errors in the velocity of the striking ship. Without sloshing the maximum penetration is higher and after the first peak it decreases and remains zero.

The total energy involved in the collision is divided into three components. These are energy E^A involved in the motions of the striking ship, energy E^B involved in the motions of the struck ship and energy E_C absorbed due to the deformation. Component E^A again consists of several energy components, as presented in Fig. 12. The work against the friction and the damping force is not presented as they were insignificant compared to the other energy components.

Fig. 12 reveals the importance of sloshing in the case of the striking ship. The energy involved in sloshing is at its maximum at the time instant when the collision force and the penetration have reached the peak values. After the maximum value, part of the sloshing energy is returned to the kinetic energy of the ship and part of it is absorbed by damping. Kinetic energy E^A_{KIN} describes the energy involved in the rigid body motions only. This energy is calculated using the total mass of the ship and the added mass of the corresponding motion component. This means that 5% of E^A_{KIN} is due to the added mass. The energy involved in sloshing, E_{SL}, is evaluated using the relative motions between the oscillating masses and the rigid body. When the effects of the sloshing are neglected, the kinetic energy of the striking ship decreases almost to zero and at the end of the contact the ship possesses significantly less energy compared to the case where the sloshing is included. As seen from the Fig. 13–15, this energy difference is absorbed by the deformation of ship structures and by the motions of the struck ship.

In the case of the struck ship, the total energy E^B is divided between more components, as the work against the damping and friction forces is more important, see Fig. 13. Also, the transformation from the sloshing energy to the kinetic energy of the ship happens faster.

According to Table 1, 24% of E^B_{KIN} is due to the added mass. That value compared to work W_K done to overcome force F_K shows the importance of the damping. In a later phase of the collision, damping energy W_K is larger than the energy involved in the motions of the added mass. Still, it should be noted that the damping energy starts to play an important role after the maximum penetration value is reached, i.e. its importance on predicting the maximum value is not very significant here. Neglecting

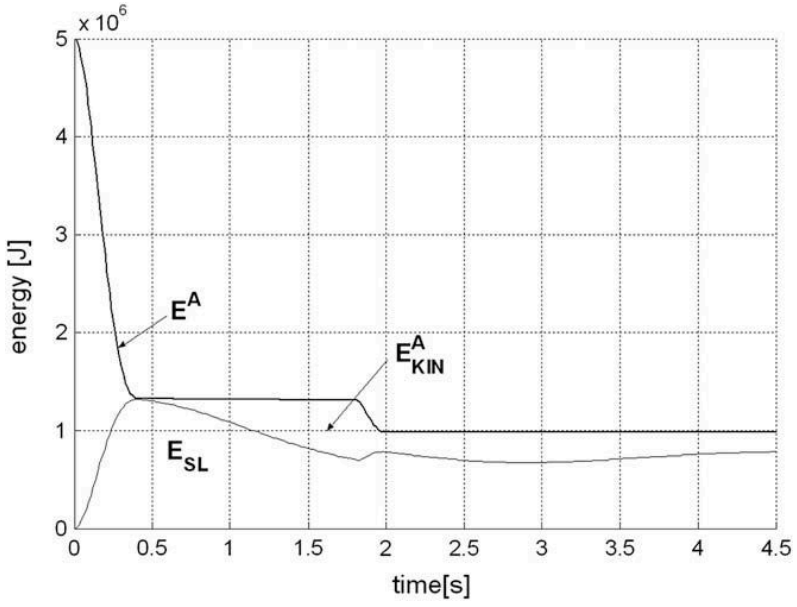

Fig. 12. Variations of relative energy components throughout the collision in the case of the striking ship (E^A total energy; E^A_{KIN} kinetic energy involved in rigid body motions; and E_{SL} energy involved in sloshing).

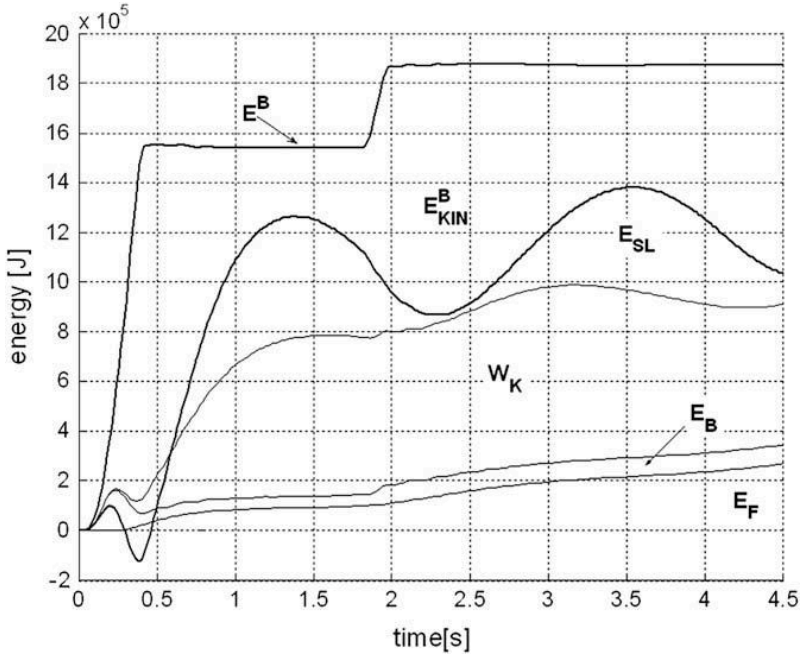

Fig. 13. Variations of relative energy components throughout the collision in the case of the struck ship (E^B total energy; E^B_{KIN} kinetic energy involved in rigid body motions; E_{SL} energy involved in sloshing; W_K work against the damping force F_K; E_B bending energy; and E_F work against the friction force).

the sloshing increases the total energy of the struck ship with the largest gain in the kinetic energy. Also the other velocity dependent energy components increase slightly as the velocity becomes higher. For simplicity, a detailed distribution of energy components for the calculations without sloshing is not presented in the figure.

Variations between E^A, E^B and E_C are presented in Fig. 14. Figure shows that only 43% of the initial energy is absorbed by the structural deformation. Energy distribution for the case where sloshing is neglected is presented in Fig. 15, which reveals that the deformation energy is 58% of the initial energy. A simple closed form method based on the momentum conservation [9] gives 65% for the relative deformation energy. This energy was calculated considering the elasticity of the ship structures, described by the relative velocity between the ships immediately after the contact is lost. The

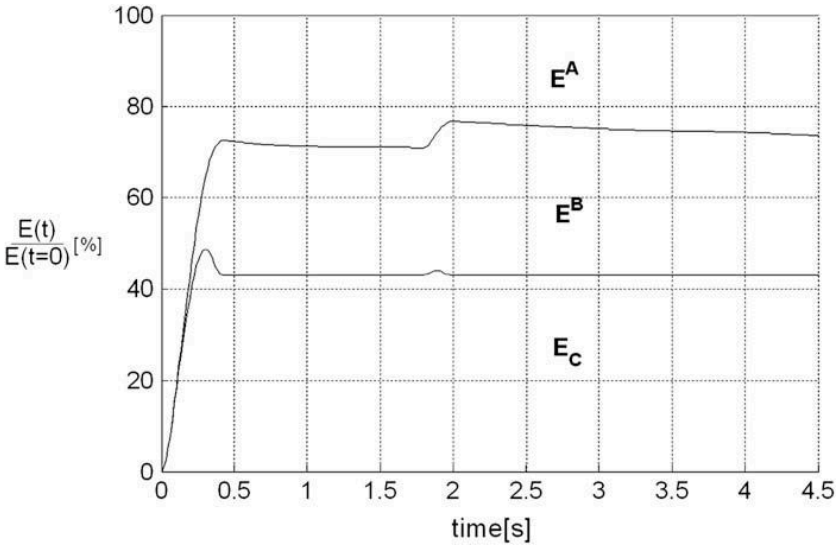

Fig. 14. Variations of relative energy components throughout the collision with sloshing effects included (E^A energy involved in the striking ship; E^B energy involved in struck ship; and E_C deformation energy).

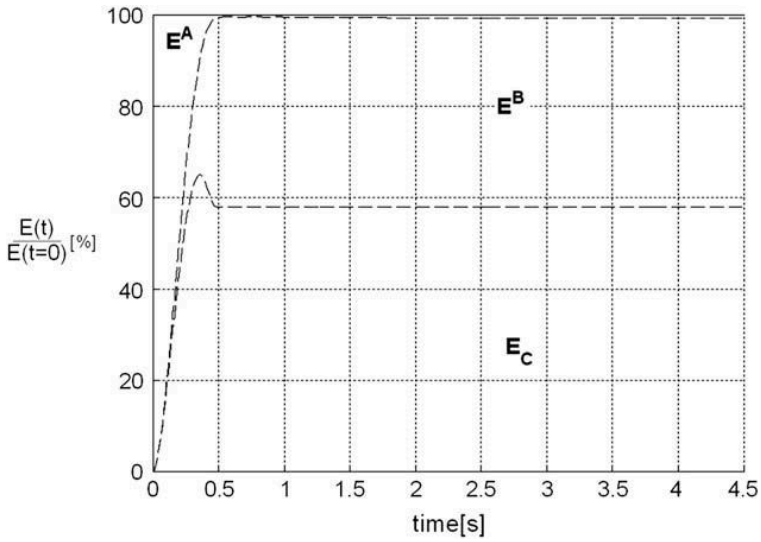

Fig. 15. Variations of relative energy components throughout the collision with sloshing effects neglected (E^A energy involved in the striking ship; E^B energy involved in struck ship; and E_C deformation energy).

differences between these results clearly indicate the importance of sloshing in the prediction of the deformation energy.

3.2. *Experiment with the* X*-core test-section*

The second example demonstrating the application of the model is the calculation of collision interaction in the experiment conducted in April 2003. The striking ship used in the test was the same as in the earlier *Y*-core test, but the struck ship was a slightly larger inland waterway barge. The effect of sloshing was removed, as only one tank in the striking ship had water ballast with a free surface. The striking ship was equipped with the same bulbous bow as in the earlier tests. The tested section was a laser welded X-type sandwich structure designed in cooperation with the EU Sandwich and EU Crashcoaster projects. Main dimensions for both ships are given in Table 2. At the moment of the first contact, the velocity of the striking ship was 3.33 m/s.

A comparison between the calculated and the measured penetration is shown in Fig. 16, which shows a good agreement, as the maximum penetration is predicted well. Again, at the later stage of the calculation, the error increased. The measured penetration started to rise again, while the calculated penetration kept decreasing slightly.

The variation of relative energy components presented in Fig. 17 differs from the *Y*-core collision. Without the sloshing water, more energy is absorbed by the deformation of the ship structures. This indicates that the sloshing water "stores" the kinetic energy of the striking ship and therefore the energy available for the deformation is decreased.

According to the momentum conservation method [9], the relative amount of the deformation energy becomes 68%. The value calculated from the experimental measurements is 75%, see Fig. 17.

Table 2
Main dimensions and loading conditions of the ships

	Striking ship	Struck ship
Length, L	80 m	76.4 m
Beam, B	8.2 m	11.4 m
Depth, D	2.62 m	4.67 m
Draft*, T	1.3 m	3.32 m
Displacement, Δ	721 tons	2465 tons
Added mass of prevailing motion component	$\mu_{11} = 0.05$	$\mu_{22} = 0.29$
Number of tanks	2×5	2×7
Ballast water with free surface	44.6 tons	0 tons

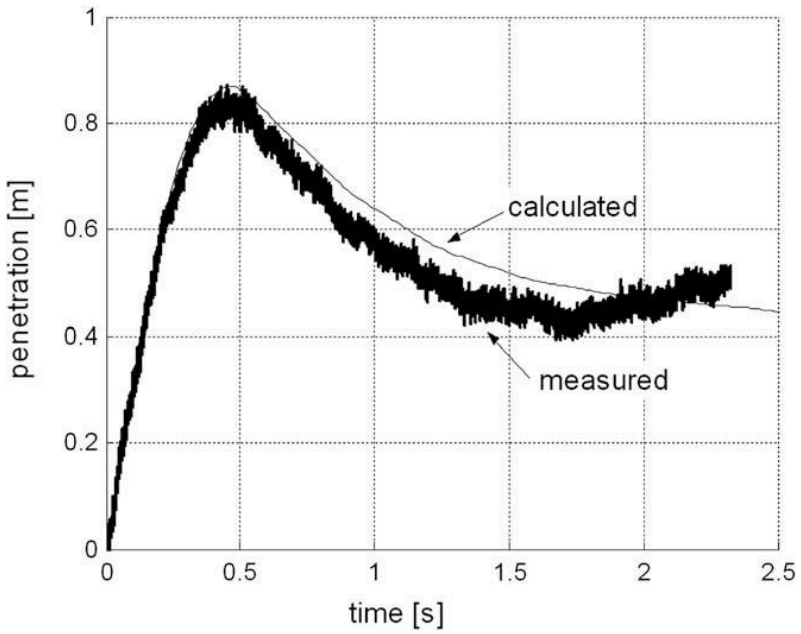

Fig. 16. Penetration as a function of time.

Larger value reveals the effect of the surrounding water, especially the part F_K of the radiation force, which is not included in the momentum conservation method. Force F_K is given with Eq. (6) and the work done to overcome this is presented as W_K in Fig. 13. This force is an additional resistance to the ship motions and can thereby be considered as an additional mass. A larger ship mass increases the inertia of the ship, and it cannot be displaced so easily.

4. Conclusion

This paper presents a model allowing for predictions of the consequences caused by the collision where large forces arise due to sloshing in ship ballast tanks. Motions of both the ships as well as the penetration depth during and after the collision were predicted in good agreement both in terms of time and absolute values. Furthermore, the vibrations of the hull girder of the struck ship corresponded

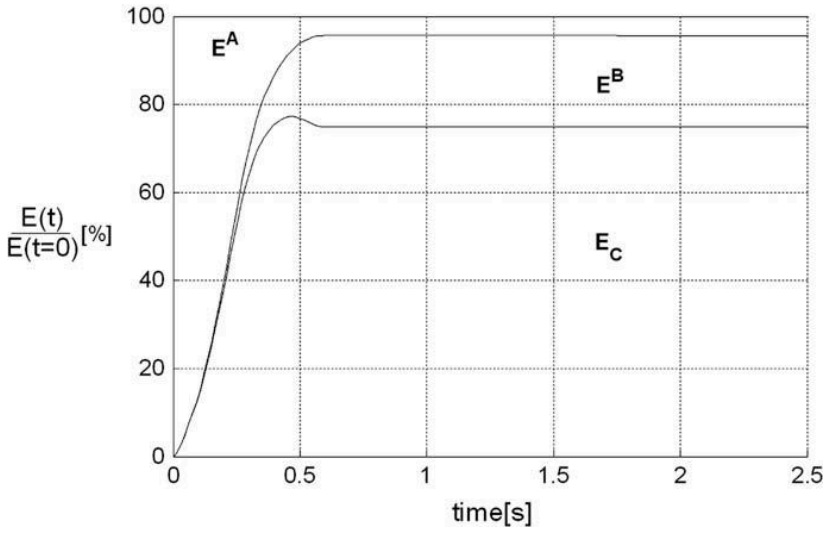

Fig. 17. Variations of relative energy components throughout the collision (E^A energy involved with the striking ship; E^B energy involved with the struck ship; and E_C deformation energy).

well with the measurements. The comparison of the energy balances revealed the significance of sloshing, as in the experiment with the sloshing effects, sloshing "stored" the kinetic energy. Therefore, only 43% of the total energy was absorbed by the structure. In the experiment without the sloshing effects, the amount of the absorbed energy was 75%. The importance of damping due to the surrounding water was large, as in the later phase of the collision, damping engaged more energy than the added mass. Damping started to play an important role after the maximum penetration value was reached.

The simplified closed form method overestimated the deformation energy with sloshing water and underestimated it without sloshing water. The closed form model needs some assumptions to be made, especially when elasticity needs to be considered. The simulation model is almost free of assumptions and only needs initial collision conditions and a collision force as a function of penetration. Therefore, the presented model is suitable for more precise collision simulations where the forces arising by the surrounding water and sloshing are to be included.

Acknowledgement

This work was carried out under the Dutch National Veilig Schip project funded by SENTER and in the framework of the Marie Curie Intra-European Fellowship program. This financial support is acknowledged.

References

[1] Minorsky VU. An analysis of ship collision with reference to protection of nuclear power plants. J Ship Res 1959;3(1):1–4.
[2] Motora S, Fujino M, Suguira M, Sugita M. Equivalent added mass of ships in collision. Selected papers from J Soc Nav Archit Japan 1971;7:138–48.
[3] Cummins WE. The impulse response function and ship motions. Schifftechnik 1962;9(47):101–9.
[4] Ogilvie TF. Recent progress towards the understanding and prediction of ship motions, fifth symposium on naval hydrodynamics. Norway: Bergen; 1964. p. 3–128.
[5] Smiechen M. Zur Kollisiondynamic von Schiffen. Jb Schiffbautech Ges 1974;68:357–72.
[6] Petersen MJ. Dynamics of ship collisions. Ocean Eng 1982;9(4):295–329.
[7] Woisin G. Instantaneous loss of energy with unsymmetric ship collisions. In: Proceedings of third international symposium on practical design of ships and mobile units (PRADS 1987). Trondheim, 1987.
[8] Pawlowski M. Energy loss in ship's collisions. Poland: Centrum Techniki Okretoewj; 1995. p. 40.
[9] Pedersen PT, Zhang S. On impact mechanics in ship collisions. Mar Struct 1998;(11):429–49.
[10] Brown A, Chen D, Sajdak JA. A simplified collision model. J Ship Res, submitted for publication.
[11] Matusiak J. Importance of memory effect for ship capsizing prediction, fifth international workshop on ship stability, 12–13 September. University of Trieste; 2001. p. 12.
[12] Journée JMJ. Strip theory algorithms. Delft University of Technology; 1992. Report MEMT 24.
[13] Kukkanen T. Two-dimensional added mass and damping coefficients by the finite element method. Report M-223. Otaniemi, Finland: Helsinki University of Technology; 1997. p. 61.
[14] Abramson, editor. Analytical representation of lateral sloshing by equivalent mechanical models, the dynamic behaviour of liquids in moving containers. NASA SP-106. Washington; 1966. p.199–223.
[15] Graham EW, Rodriguez AM. The characteristics of fuel motion which affect airplane dynamics, Trans. Of ASME, Series E. J Appl Mech Sept 1952;19(no.3):381–8.
[16] Hirt CW, Nichols BD. Volume of fluid (VOF) method for the dynamics of free boundaries. J Comput Phys 1981;39:201–25.
[17] Timoshenko SP. Vibration problems in engineering. 2nd ed. New York: D. Van Nostrand Company Inc.; 1937. p. 470.
[18] Glough RW, Penzien J. Dynamics of structures. 2nd ed. New York: McGraw-Hill Book Company; 1993. p. 740.
[19] ISSC. Steady state loading and response, report of committee II.4. Proceedings of the eighth international ship structures congress; 1983. p. 64.
[20] Wevers LJ, Vredeveldt AW. Full scale ship collision experiments 1998, TNO. report 98-CMC-R1725. The Netherlands: Delft; 1999. p. 260.